Clustering of cyclic-nucleotide-gated channels in olfactory cilia

Richard J. Flannery[*], Donald A. French[†], and Steven J. Kleene[*]
[*]Department of Cell Biology, Neurobiology, and Anatomy
[†]Department of Mathematical Sciences
University of Cincinnati
Cincinnati, OH 45267, USA

Address correspondence to:

Steven J. Kleene
Department of Cell Biology, Neurobiology, and Anatomy
University of Cincinnati
PO Box 670667
Cincinnati, OH 45267-0667, USA

513-558-6099
513-558-2727 FAX
steve@syrano.acb.uc.edu

Running title: CNG channel clusters in olfactory cilia

Key words: olfaction, receptor neuron, cyclic-nucleotide-gated channel, sensitivity, patch-clamp, electrophysiology

ABSTRACT

Olfactory cilia contain the known components of olfactory signal transduction, including a high density of cyclic-nucleotide-gated (CNG) channels. CNG channels play an important role in mediating odor detection. The channels are activated by cAMP, which is formed by a G-protein-coupled transduction cascade. Frog olfactory cilia are 15 to 200 μm in length, so the locations of CNG channels along the length may be important in determining the sensitivity of odor detection. We have recorded from excised cilia and modeled diffusion of cAMP into a cilium in order to determine the locations of the CNG channels along the ciliary length. The proximal segment, which is the first 20% of the cilium, appears to express a low density of CNG channels, while the distal segment contains a high density of channels, mostly clustered in one region. This is consistent with a previous electron micrographic study that found CNG channels to be primarily located in distal segments.

INTRODUCTION

Olfactory signal transduction primarily occurs on the olfactory cilia, which extend from the tip of the dendritic knob of olfactory receptor neurons (~01). The cilia contain molecules required for transduction of an odor stimulus, including odorant receptor proteins, the G-protein G_{olf}, CNG and Cl^- channels, adenylate cyclase III, cAMP phosphodiesterase, and two transduction channels (~01,~02). One of these, a cyclic-nucleotide-gated (CNG) channel, is gated by cAMP and conducts a depolarizing cationic current into the cilia. CNG channels are expressed at high densities in olfactory cilia (~03,~04,~05,~06). Cilia increase the neuron's ability to detect odorant molecules by extending into the mucus and by increasing the surface area of the sensory neuron by about 40 times (~02). Typically a cilium's length is about 100 times its diameter. This geometry may be ideal for increased binding of odor molecules to the surface, but it may also lead to unique challenges for transducing signals after an odor molecule binds. A consequence of the unique geometry is the limited diffusion of second messengers (~07). It has been shown in other cell types that cAMP and CNG channels interact within and are restricted to domains, partly due to limited diffusion of cAMP (~08,~09).

The distribution of CNG channels along the length of the cilium should be an important determinant of neuronal sensitivity. However, the distribution itself remains controversial. An electrophysiological study indicated that the channels are uniformly distributed along the length of the cilium (~10). In that study, the length of cilium illuminated to release caged cAMP was linearly related to the total current generated, suggesting that CNG current-generating capacity is

uniformly distributed. However, immunohistochemical studies of channels in olfactory cilia indicated that channels are expressed more prominently in distal regions (~11). Models of olfactory neuron function have assumed that ion channels are distributed uniformly (~07,~12,~13,~04,~05).

We have used a computational model to interpret patch-clamp experiments, in order to determine where the CNG channels are located along the ciliary length. Our results show that distal segments contain the majority of the CNG channels, and these channels tend to be clustered in one region. Our results are consistent with the imaging studies that found that found higher expression of CNG channels in distal regions than in proximal regions.

METHODS

Ciliary Patch Procedure

Electrical recordings were made from olfactory cilia of Northern grass frogs (*Rana pipiens*) as described elsewhere (~14). Frog olfactory epithelium was dissociated by mechanical shredding. One cilium of an isolated olfactory receptor neuron was drawn into a patch pipette, and a high-resistance seal was made where the olfactory knob meets the base of the cilium. The cilium was then excised from the cell, resulting in an inside-out patch configuration. The pipette containing the cilium was moved to a pseudointracellular bath so that the intracellular side of the cilium was exposed to the bath solution. The cilium was then transferred to baths containing various

concentrations of cAMP. Contact with the solution in these wells initiated the diffusion of cAMP into the cilium. The resulting CNG channel activation was recorded over a period of approximately 4 s. Maximal channel activity was typically achieved after approximately 1-2 s. Multiple concentrations of cAMP were tested for each cilium, including 300 μM, which quickly gave a saturating current. The patch procedure was videotaped, and ciliary lengths were estimated by playing back the video images one frame at a time.

The extracellular (pipette) solution contained (in mM): NaCl, 115; KCl, 3; Na_3-EDTA, 1; Na-HEPES, 5; pH 7.2. The pseudointracellular (bath) solution contained (in mM): NaCl, 110; KCl, 5; K_4-BAPTA, 2; K-HEPES, 5; pH 7.2. Both solutions were free of divalent cations. This eliminated the possibility that Ca^{2+} might enter the cilium and activate a Cl^- current (~15,~16). With these solutions, the cAMP-activated current reversed at 0 mV.

Modeling

Two versions of the biophysical model were employed in our study: a forward version and an inverse solution. The inverse solution was done first, generating a channel density function from an experimental record of current vs. time. The accuracy of the density function was then assessed by using the density function as input for the forward model. The forward model makes predictions about the time course of the current through the CNG channels, given an ion channel density function. The predicted current was compared to the experimental result. The model easily discriminates between uniform and step distributions of channels (~17). In all figures, 0 represents the proximal end of the cilium (i.e. the end that contacts the basal body).

Forward biophysical model

A computational model was used to make predictions about channel currents resulting from diffusion of cAMP into a cilium, given a particular ion channel density function (for example Fig. 2). The model accounted for several physical processes, including diffusion of cAMP, binding of cAMP to the CNG channels, channel activation, and cable-conduction effects. Diffusion and binding of cAMP were modeled by a nonlinear time-dependent partial differential equation which also depends on the channel distribution, $\rho(x)$. Membrane potential satisfies a second-order boundary value problem which depends on ρ and the concentration of cAMP. These equations are approximated by basic finite difference schemes. A more detailed description of this model is given in French et al. (~17).

Some minor considerations were not included in the model. It does not account for a small leak conductance in the ciliary membrane (~18). Only experiments with minimal leak conductance (input resistance $\geq$ 1 GΩ) were used. The model also assumes that the cilium is a cylinder of constant diameter. In fact, the diameter decreases abruptly from 0.28 μm to 0.19 μm where the proximal and distal segments meet (~19). The tapering of the cilium is not expected to slow diffusion significantly. It is assumed that unhindered diffusion is possible in the entire volume of the cilium, as suggested by Chen et al. (~13). Finally, capacitative current has been ignored. We estimate that the time constant of a cilium should be ~3 ms, which is much faster that the events recorded here.

Inverse solution

The primary unknown in our biophysical model was the locations of the CNG channels, and it was the aim of our modeling and experiments to generate a function quantifying this unknown. The inverse solution offers a systematic way of generating density functions, using the measured time-dependent activation of CNG channels as input. The inverse solution has the same components as those described in the forward biophysical model, as well as a Fredholm integral equation which has a kernel that depends on the membrane potential and concentration of cAMP. Through a series of iterations, the inverse solution makes an approximation of the density function, $\rho(x)$. The inverse solution is described in greater detail in French et al. (~17).

The noisy raw current data were smoothed by a moving average with 11 points and then used to generate an inverse solution (a current density function ρ). For this approximation, the smoothed raw data were averaged over $N = 20$ intervals of length T/N, where T is the duration of the recording. This yielded a set of 21 discrete current values. To evaluate the inverse solution, the current density function was converted back to a predicted current by solving a forward problem. Using the piecewise constant ρ function, a discrete cAMP concentration and membrane potential were computed using finite differences. Discrete current values were then produced at 21 points in time.

Selection of data

About 70% of the density functions were judged to be credible. The remaining 30% were rejected. In some of these, the model reported an unrealistically high number of channels, often

with all channels located at the proximal or distal end of the cilium. Based on an unpublished analysis of a study of 117 cilia (~05), we decided to reject solutions that predicted >40,000 channels for a cilium. On other occasions, the inverse solution did not converge. In those cases, results were discarded after checking with the forward model. Ideally the forward model should convert the inverse solution (a density function) to a current record the same as the experimental record in every respect except noise (Fig. 2 *A*). If these two curves are different, the density function is inaccurate. Differences between the curves were measured as the difference between the areas under the curves. This is known as the residual value, and it was used to determine whether results should be discarded. In such cases, the inverse solution appeared to be making poor initial guesses that could not be rectified during subsequent iterations. After some practice, it was always possible to design a density function by trial and error such that providing the function as input to the forward model accurately predicted the experimental recording. However, all of the density functions shown were produced as inverse solutions rather than by trial and error.

Sensitivity Analysis

Nine experimentally determined values were treated as constants in the model (Table 1), but most of these were associated with measured experimental errors. By doing sensitivity analysis, we determined how errors in the constants affected the channel density functions inferred from the model. A range of values for each of four of the constants (D, g_{CNG}, n, and $K_{1/2}$) were used to generate multiple density functions for a single cilium. For each constant, the maximum and

minimum values equalled the mean value plus or minus one standard error or one standard deviation as shown in Table 1. Five values for each constant were used, including the mean, the maximum and minimum values, and two other values equidistant between the maximum and mean or minimum and mean. For the four constants tested, this resulted in $5^4 = 625$ density functions.

RESULTS

When a cilium was placed in a bath containing cAMP, there was a short delay, or a period of CNG current activation with a relatively shallow slope, after which the current increased more rapidly. For one 100-μm cilium, the delay was 200 ms in 10 μM cAMP (Fig. 1 *A*) and 70 ms in 300 μM cAMP (Fig. 1 *B*). Longer delays were seen with longer cilia and lower [cAMP] (Table 2). Without regard to length of the cilium, the average delays in 10 μM cAMP and 300 μM cAMP were 78 and 39 ms, respectively.

Following the delay, the cAMP-activated current increased rapidly, reaching a maximum after 200 ms or longer, again depending on [cAMP] and length of the cilium. The time to reach maximum current was longer when longer cilia or lower [cAMP] were used. The maximum current value was highly variable. There is no correlation between ciliary length and maximum current (~05). In the model, the initial phase of current activation primarily determined the

proximal channel patterns, whereas the slope of the second phase was the primary determinant for distal channel patterns.

One 70-μm cilium reached a maximum current of 100 pS after approximately 1 s (Fig. 2 *A*). Six such experiments were performed with this cilium, using cAMP concentrations of 10 or 20 μM. For each experiment, the inverse solution was used to generate a density function for this cilium. Three of the density functions for this cilium are shown in Fig. 2 *B-D*. These density functions have common features. Usually most of the channels were clustered in one small region about 5 to 10 μm wide. This primary cluster appeared in density functions from each trial using the same cilium, regardless of cAMP concentration. In some individual trials (e.g. Fig. 2 *B*), smaller clusters appeared. When all 6 density functions for this cilium were averaged (Fig. 3 *A*), the smaller clusters disappeared or appeared as shoulders in the main peak.

Averaged density functions for 3 cilia are show in Fig. 3 *A-C*. In each averaged density function, there was one major cluster 15 to 20 μm wide in the distal segment. A smaller cluster appeared near the base of the cilium, and this cluster was more prominent in some cilia (e.g. Fig. 3 *C*). At least 2 concentrations of cAMP were used for each cilium. Typically these included a saturating dose, usually 300 μM, and a low dose, between 1 and 10 μM. In most cases, density functions from experiments using low and high concentrations were similar.

The clustering of CNG channels was apparent even when density functions from 35 cilia were averaged (Fig. 4 *A*). To facilitate comparisons among the 35 cilia, ciliary length and number of

channels were normalized. For all cilia, the average distance from the base for the primary ion channel clusters was 33% of the length of the cilium. This should be in the distal segment of the cilium (Fig. 4 *B*).

Accumulation of sodium

Our model assumes that the concentration of the current-carrying ion (Na^+) is equal and constant on both sides of the ciliary membrane. It was conceivable, though, that the influx of Na^+ during the experiment might cause an accumulation of Na^+ within the tiny volume of the cilium (~20). To test this, voltage was applied instantaneously to a cilium already filled with a saturating concentration of cAMP. Maintaining this voltage led to just a small decrease in the driving force for Na^+. In Fig. 5, the total current decreased from –474 pA to –450 pA over 1 s, reflecting a 5% decrease in the driving force for Na^+ into the cilium. There was no effect on the driving force for Na^+ in the absence of cAMP (Fig. 5).

Sensitivity Analysis

Values treated as constants in the model were determined experimentally, but many of these were associated with measured experimental errors (Table 1). By doing sensitivity analysis, we were able to determine how errors in the constants generated variability in the predictions of the model.

For each of 4 constants, 5 values were assumed as described in "Materials and Methods". First a density function was generated using the mean value of each constant (Fig. 6 *A*). Then each of

the 625 permutations of values was used to generate a channel density function. These functions were averaged, and the standard errors for the number of channels at each position in the 625 density functions were calculated (Fig. 6 *B*). The standard errors and channel densities are highest at the same positions (Fig. 6 *A,B*). This indicates there was variability in the number of channels reported by the model, but little variability in the locations of the channels. Inspection of the individual 625 density functions (not shown) revealed that changes in the values of the constants resulted in movement of the primary peak in the density function by a maximum of 4% of the total length. Smaller peaks appearing in the distal region were highly variable and often appeared at 45 μm or 55 μm in this 70-μm cilium.

The mathematical model assumes that diffusion of cAMP is limited by binding to sites on the CNG channels. The number of binding sites per channel assumed (Fig. 7) had little effect on the channel distribution reported by the model.

DISCUSSION

As cAMP diffuses into a cilium, it activates a current with a distinctly biphasic time course (Fig. 1). There is a short period of time during which little or no current appears, followed by a rapid activation of current. Diffusion time is proportional to the square of the distance diffused. Therefore diffusion over short distances is very much more rapid than diffusion over longer distances. The initial slow activation of channels indicates that there is some distance at the base

of the cilium where the channel density is very low. The inverse mathematical model uses information from both phases of the recording to generate a channel density function which accounts for the experimental results. Although the results varied among cilia, several trends in channel expression were apparent and were quantified in this study.

The channel distributions can be conveniently discussed by referring to the two ciliary segments defined by morphological studies (Fig 4 *B*). In frog, the proximal segment is roughly that 20% of the cilium nearest the cell body (~21). The proximal segment has a diameter of 0.28 μm (~19), and its axoneme has a full (9 × 2) + 2 complement of microtubules (~21, ~19). The remaining 80% of the cilium is the distal segment, which has a diameter of 0.19 μm (~19). Microtubules in the distal segment are single rather than paired; in the frog the most common configuration is (9 × 1) + 2 (~21).

We found that the proximal and distal segments each contain one region with a higher density of CNG channels and a second region with a lower density of channels. The half of the proximal segment nearest the basal body (i.e. the first 10% of the ciliary length) contained 10.2% of the channels (Fig. 4). The channels attributed to this part of the cilium may include some channels from the dendritic knob. It is likely that an excised cilium retains a small portion of the dendritic knob. The dimensions of the pipette tip (diameter 0.5 μm) and the knob (diameter 1-2 μm) determine that the length of dendritic knob contributing to our recordings is < 1 μm. Membranes excised from the dendrite do contain some CNG channels (~06), although many more are found

in the cilia. The remainder of the proximal segment (i.e. the next 10% of the ciliary length) contained just 1.5% of the channels.

The first half of the distal segment (40% of the ciliary length) contained 81.9% of the total CNG channels. This region had an average channel density twice as great as that in the first proximal region. The remainder of the distal segment, which is the 40% of the cilium farthest from the basal body, contained just 6% of the channels. Our results are consistent with a localization of the CNG channel subunit CNGA2 in rat by immunoelectron microscopy (~11). In that study, the majority of the immunoreactivity was in the distal segments of the cilia. In addition, we have now shown how channel expression varies along the length of the distal segment and demonstrated that the distal channels are functional.

In an earlier electrophysiological study, Lowe and Gold (~10) concluded that CNG current-generating capacity is uniformly distributed along the length of the cilium. When caged cAMP within cilia was photolyzed, the length of cilium illuminated was linearly related to the total current generated. This result is inconsistent with those presented here and by Matsuzaki et al.(~11). A possible explanation for the inconsistency is that in Lowe and Gold's experiments, cAMP is diffusing toward the channels following photolysis of caged cAMP. Also, it is now recognized that Lowe and Gold were undoubtedly measuring a sum of currents through both CNG and Ca^{2+}-activated Cl^{-} channels. The spatial distribution of the Cl^{-} channels is still unknown.

We used an inverse solution of a mathematical model to infer the spatial distribution of the CNG channels. This solution has a very high condition number, suggesting that many solutions exist which could account for the experimental result. In other words, many density functions, when used as input to the forward biophysical model, will produce the same predicted current. However, our results demonstrate that while there may be many solutions, these solutions have both qualitative and quantitative features which are highly reproducible. These features include: 1) a short region near the base of the cilium where no functional channels exist, 2) a short region in the distal segment which contains the majority of the channels, and 3) a larger region at the distal end which has few functional channels. Other features were moderately to highly variable. These features include the total number of channels and the appearance of minor clusters of channels in very distal regions. Modeled predictions of the number of channels in far distal regions were expected to be somewhat variable due to the slower rate of diffusion and the smaller currents from these channels due to cable-conduction loss. For these reasons, the model is not as sensitive to small changes in channel densities in the far distal regions.

Nine experimentally determined values were treated as constants in the model (Table 1), but each of these values was associated with a measured experimental error. Sensitivity analysis of four of these constants (Fig. 6) revealed that the clustering of channels was observed over reasonable ranges for these constants. We would not have predicted this in all cases. It was surprising, for example, that binding of cAMP to the CNG channels had little effect on the inferred channel distributions (Fig. 7). A model 50-μm cilium filled with 10 μM cAMP should contain ~14000 molecules of cAMP. If a cilium has 2500 CNG channels (~03), each with 4

cAMP-binding sites (~22), diffusion of cAMP should be significantly slowed by this binding. In fact, though, this binding did not influence the channel distribution reported by the model.

It is not clear yet why functional channels are rare in the most distal 40% of the cilium. In chemosensory cilia of *Caenorhabditis elegans*, intraflagellar transport (IFT) is required for expression of some transduction channels in the distal segment (~29). The distal segment of the frog cilium has an incomplete axoneme (~21), and one could imagine that this prevents the CNG channels from being transported toward the distal tip. However, two facts make this explanation unlikely. First, on average the highest density of CNG channels was found 33% down the length of the cilium (Fig. 4). This is already within the distal segment, assuming the distal segment is 80% of the cilary length (~21). Second, IFT of axonemal components occurs even in distal ciliary segments where the axoneme is composed of singlet tubules (~30). It is possible that channels in the farthest distal regions of cilia lose their functionality because they are exposed to a relatively unregulated external environment .

Channel clustering is a phenomenon observed in many cell types and neuronal compartments, including neuronal axons, hair cells of the inner ear (~23,~24), and pancreatic beta cells (~25). The functions of channel clustering include regulation of oscillation frequency in hair cells and neurosecretory cells, as well as compartmentalization of signaling components in neuronal synapses. In olfactory cilia, clustering of CNG channels may be part of a system that enhances the efficiency of signal transduction. Odor transduction in cilia is initiated by an odor molecule binding to a G-protein-coupled receptor, which results in the formation of cAMP. cAMP then

activates the CNG channels, and Ca^{2+} entering through the CNG channels gates Ca^{2+}-activated Cl^{-} channels (reviewed in ref. ~01). A concentration of these components should enhance the efficiency of transduction. For example, cAMP may be hydrolyzed by a phosphodiesterase before it diffuses to a CNG channel. If the site of cAMP synthesis is close to a channel, channel activation may be favored over cAMP hydrolysis. Concentration of transduction components could also facilitate the amplifying function of the Cl^{-} channels. Intracellular Ca^{2+} concentration is expected to reach higher values near Ca^{2+} channel clusters (~26) such as the CNG channel clusters we observed. A higher Ca^{2+} concentration should result in greater activation of Cl^{-} channels. The higher concentration of Ca^{2+} that results from CNG channel clustering will result in a higher ratio of Cl^{-}/CNG channel activity, which is optimal for maximizing the signal-to-noise ratio of the receptor current (~03). Although most of the molecules of olfactory transduction are concentrated in the distal segment of the cilium (~02), it is not known if they are particularly localized to the smaller domain where the CNG channels are clustered. Transduction could be improved by grossly concentrating the proteins within such a 10- to 15-μm length of the cilium. Furthermore, the proteins may be concentrated at the molecular level within microdomains (~31,~32).

ACKNOWLEDGMENTS

We are grateful to Bill Krantz and Chuck Groetsch for helpful discussions, and to Tom Nickell and Bert Menco for critical reviews of the manuscript. This work was supported by research

grants F31 DC006121 to R.J.F and R01 DC00926 to S.J.K from the National Institute on Deafness and Other Communication Disorders, National Institutes of Health, and grant DMS-0515989 to D.A.F. and S.J.K from the Division of Mathematical Sciences, National Science Foundation.

REFERENCES

~01. Schild, D., and D. Restrepo. 1998. Transduction mechanisms in vertebrate olfactory receptor cells. *Physiol. Rev.* 78:429-466.

~02. Menco, B.Ph.M. 1997. Ultrastructural aspects of olfactory signaling. *Chem. Senses*. 22:295-311.

~03. Kleene, S.J. 1997. High-gain, low-noise amplification in olfactory transduction. *Biophys. J.* 73:1110-1117.

~04. Larsson, H.P., Kleene, S.J., and Lecar H. 1997. Noise analysis of ion channels in non-space-clamped cables: Estimates of channel parameters in olfactory cilia. *Biophys. J.* 72:1193-1203.

~05. Kleene, S.J., Gesteland, R.C., and Bryant, S.H. 1994. An electrophysiological survey of frog olfactory cilia. *J. Exp. Biol.* 195, 307-328.

~06. Kurahashi, T., and Kaneko, A. 1993. Gating properties of the cAMP-gated channel in toad olfactory cells. *J. Physiol.* 466:287-302.

~07. Lindemann, B. 2001. Predicted profiles of ion concentrations in olfactory cilia in the steady state. *Biophys. J.* 80:1712-1721.

~08. Karpen, J.W., and Rich, T.C. 2004. Resolution of cAMP signals in three-dimensional microdomains using novel, real-time sensors. *Proc. West. Pharmacol. Soc*. 47:1-5.

~09. Karpen, J.W., and Rich., T.C. 2005. High-resolution measurements of cyclic adenosine monophosphate signals in 3D microdomains. *Methods Mol. Biol*. 307:15-26.

~10. Lowe, G., and Gold, G.H. 1991. The spatial distributions of odorant sensitivity and odorant-induced currents in salamander olfactory receptor cells. *J. Physiol*. 442:147-168.

~11. Matsuzaki, O., Bakin, RE., Cai, X., Menco, B.Ph.M., and Ronnett, G.V. 1999. Localization of the olfactory cyclic nucleotide-gated channel subunit 1 in normal, embryonic and regenerating olfactory epithelium. Neuroscience 94:131-140.

~12. Reisert, J., Bauer, P.J., Yau, K.-W., and Frings, S. 2003. The Ca-activaed Cl channel and its control in rat olfactory receptor neurons. *J. Gen. Physiol*. 122:349-363.

~13. Chen, C., Nakamura, T., and Koutalos, Y. 1991. Cyclic AMP diffusion coefficient in frog olfactory cilia. *Biophys. J*. 76:2861-2867.

~14. Kleene, S.J., and Gesteland, R.C. 1991. Transmembrane currents in frog olfactory cilia. *J. Membr. Biol*. 120:75-81.

~15. Kleene, S.J. 1993. Origin of the chloride current in olfactory transduction. *Neuron.* 11:123-

132.

~16. Kurahashi, T., and K.W. Yau. 1993. Co-existence of cationic and chloride components in odorant-induced current of vertebrate olfactory receptor cells. *Nature.* 363:71-74.

~17. French, D.A., Groetsch, C.W., Krantz, W.B., Flannery, R., and Kleene, S.J. 2005. Numerical approximation of solutions of a nonlinear inverse problem arising in olfaction experimentation. Manuscript submitted.

~18. Kleene, S.J. 1992. Basal conductance of frog olfactory cilia. *Pflügers Arch.* 421:374-380.

~19. Menco, B.Ph.M. 1980. Qualitative and quantitative freeze-fracture studies on olfactory and nasal respiratory structures of frog, ox, rat, and dog. *Cell Tissue Res.* 207:183-209.

~20. Zimmerman, A.L., Karpen, J.W., and Baylor, D.A. 1988. Hindered diffusion in excised membrane patches from retinal rod outer segments. *Biophys. J.* 54:351-355.

~21. Reese, T.S. 1965. Olfactory cilia in the frog. *J. Cell Biol*. 25:209-230.

~22. Kaupp, U.B., and R. Seifert. 2002. Cyclic nucleotide-gated ion channels. *Physiol. Rev.* 82:769-824

~23. Rispoli at el., 2001

~24. Roberts, 1999

~25. reference(s) for pancreatic beta cells

~26. Shuai, J.W., and Jung, P. 2002. Optimal intracellular calcium signaling. *Phys. Rev. Lett.* 88:068102.

~27. Kleene, S.J. 1999. Both external and internal calcium reduce the sensitivity of the olfactory cyclic-nucleotide-gated channel to cAMP. *J. Neurophysiol*. 81:2675-2682.

~28. Bowen, W.J., and Martin, H.L. 1964. The diffusion of adenosine triphosphate through aqueous solutions. *Arch. Biochem. Biophys*. 107:30-36.

~29. Qin, H., Burnette, D.T., Bae, Y.-K., Forscher, P., Barr, M.M., and Rosenbaum, J.L. 2005. Intraflagellar transport is required for the vectorial movement of TRPV channels in the ciliary membrane. Curr. Biol. 15:1695-1699.

~30. Snow, J.J., Ou, G., Gunnarson, A.L., Walker, M.R., Zhou, H.M., Brust-Mascher, I., and Scholey, J.M. 2004. Two anterograde intraflagellar transport motors cooperate to build sensory cilia on *C. elegans* neurons. *Nat. Cell Biol*. 6:1109-13.

~31. Paysan, J., and Breer, H. 2001. Molecular physiology of odor detection: current views. *Pflügers Arch*. 441:579-586.

~32. Brady, J.D., Rich, T.C., Le, X., Stafford, K., Fowler, C.J., Lynch, L., Karpen, J.W., Brown, R.L., and Martens J.R. 2004. Functional role of lipid raft microdomains in cyclic nucleotide-gated channel activation. *Mol. Pharmacol*. 65:503-11.

TABLE 1 Constants used in the model

Constant	Value	References
$K_{1/2}$	1.70 ± 0.19 μM (SEM)	~27
Hill constant, n	1.70 ± 0.07 (SEM)	unpublished data from ref. ~27
Single-channel conductance, g_{CNG}	8.3 ± 2.3 pS (SD)	~04
Maximum open probability, P	0.70 ± 0.095 (SD)	~04
Reversal potential of CNG channel	0 mV	
cAMP binding sites	1 / channel	
Ciliary diameter, d	0.28 ± 0.03 μm (SD)	~19
cAMP diffusion coefficient, D	3.3×10^{-6} cm^2 s^{-1}	~28
Intracellular axial resistance, r_a	1.5×10^{11} Ω cm^{-1}	

Terminology is as in French et al. (~17). $K_{1/2}$ is the concentration of cAMP that gives half-maximal activation of the CNG channel. The value of r_a corresponds to an intracellular resistivity R_i of 92 Ω cm, i.e. the resistivity of 115 mM NaCl assuming the ciliary diameter shown. The diffusion coefficient is the minimum value determined for ATP (~28). A similar value (2.7×10^{-6} cm^2 s^{-1}) was measured for cAMP in olfactory receptor neurons (~13).

TABLE 2 Delays in activation of CNG current

	Current delay (ms)	
length of cilium	[cAMP] = 10 μM	[cAMP] = 300 μM
40 μm	42 ± 9 (*n* = 6)	20 ± 5 (*n* = 6)
70 μm	52 ± 11 (*n* = 6)	22 ± 2 (*n* = 6)
100 μm	131 ± 11 (*n* = 7)	69 ± 4 (*n* = 7)

The time (as mean ± SEM) is shown between immersion of the cilium in cAMP and the onset of the rapidly increasing current. Each row lists repeated measurements from a single cilium. The first row is from the same cilium used for Fig. 1.

FIGURE LEGENDS

FIGURE 1 Time courses of CNG current activated by placing a 100-μm cilium in 10 μM cAMP (*A*) and then 300 μM cAMP (*B*). At the start of each recording, the cilium was in a cAMP-free bath and showed a leak current of ~25 pA. The cilium was briefly moved through the air, during which time the current was 0 pA. At the time indicated by the *arrow*, the cilium was immersed in a bath containing cAMP. Initially this activated a current with a slow rise and a very low amplitude (0 to 5 pA after subtraction of the leak current). This was followed by a current with a steeper slope that began approximately 200 ms (*A*) or 70 ms (*B*) after immersion in the cAMP-containing bath. Membrane potential was clamped at –50 mV throughout the experiment.

FIGURE 2 *A*, The recording with fluctuations shows the current measured after a 70-μm cilium was immersed in cAMP. Given this recording, an inverse solution of the channel density function (*B*) was generated with the mathematical model. A forward calculation from this density function (*B*) predicted the current shown as *open circles* in *A*. The experiment was repeated with this cilium 6 times. *B*, *C* and *D* are the predicted density functions from 3 of these experiments. The concentration of cAMP was 10 μM (*A,B,D*) or 20 μM (*C*).

FIGURE 3 Density functions were generated from multiple experiments using the same cilium and these were averaged and normalized. Average density functions are shown for 6 experiments with a 70-μm cilium (*A*), 7 experiments with a 40-μm cilium (*B*), and 5 experiments with a 50-μm cilium (*C*). *A* is from the same 70-μm cilium as in Fig. 2. Clusters of channels

sometimes appeared in the proximal region, and this is prominent in *C*. In this and subsequent figures, the error bars represent the SEM.

FIGURE 4 *A*, Average CNG channel density functions from 35 different cilia. For each cilium, density functions were determined in 1 to 7 experiments. Those were averaged to get an average density function for that cilium. Those 35 average functions were again averaged to produce the result shown. Of the 35 experiments, 6 used 3.5 μM cAMP or less, 10 μM was used for 35 experiments, 20 μM was used for 8, and 100 μM or greater was used for 10 experiments. *B*, schematic of an olfactory cilium showing the proximal and distal segments, plus a piece of the dendritic knob at the far left. The relative diameters are drawn to scale. The length is scaled to match the distance axis in *A*.

FIGURE 5 Test for a change in driving force during a sustained Na^+ current. In the recording shown in *black*, a cilium was immersed in a bath containing 300 μM cAMP. Voltage was clamped at 0 mV to eliminate any Na^+ current. At time 0, the membrane potential was changed to −50 mV. The Na^+ current reached a maximum value and then decreased slightly. No change in driving force was detectable when the experiment was repeated in a cAMP-free bath (recording shown in *gray*).

FIGURE 6 Sensitivity analysis of the model. Four constants used in the model (Hill coefficient n, $K_{1/2}$ for activation of CNG channels by cAMP, diffusion coefficient of cAMP, and unitary conductance of the CNG channel) were varied in the model. *A*, channel density function

obtained using the mean values (Table 1). *B*, 625 channel density functions were generated by varying the values of the 4 constants as described in "Materials and Methods". These 625 density functions were averaged. The SEM of the number of channels at each point along the cilium is plotted.

FIGURE 7 The modeled extent of cAMP binding to the CNG channels has little effect on the inferred channel distributions. *A*-*E*, averaged density functions from 35 cilia in which each CNG channel was assumed to have 0, 1, 2, 3, or 4 cAMP-binding sites. All of the averaged density functions show roughly the same CNG channel locations. *B* is the same result shown in Fig. 4.

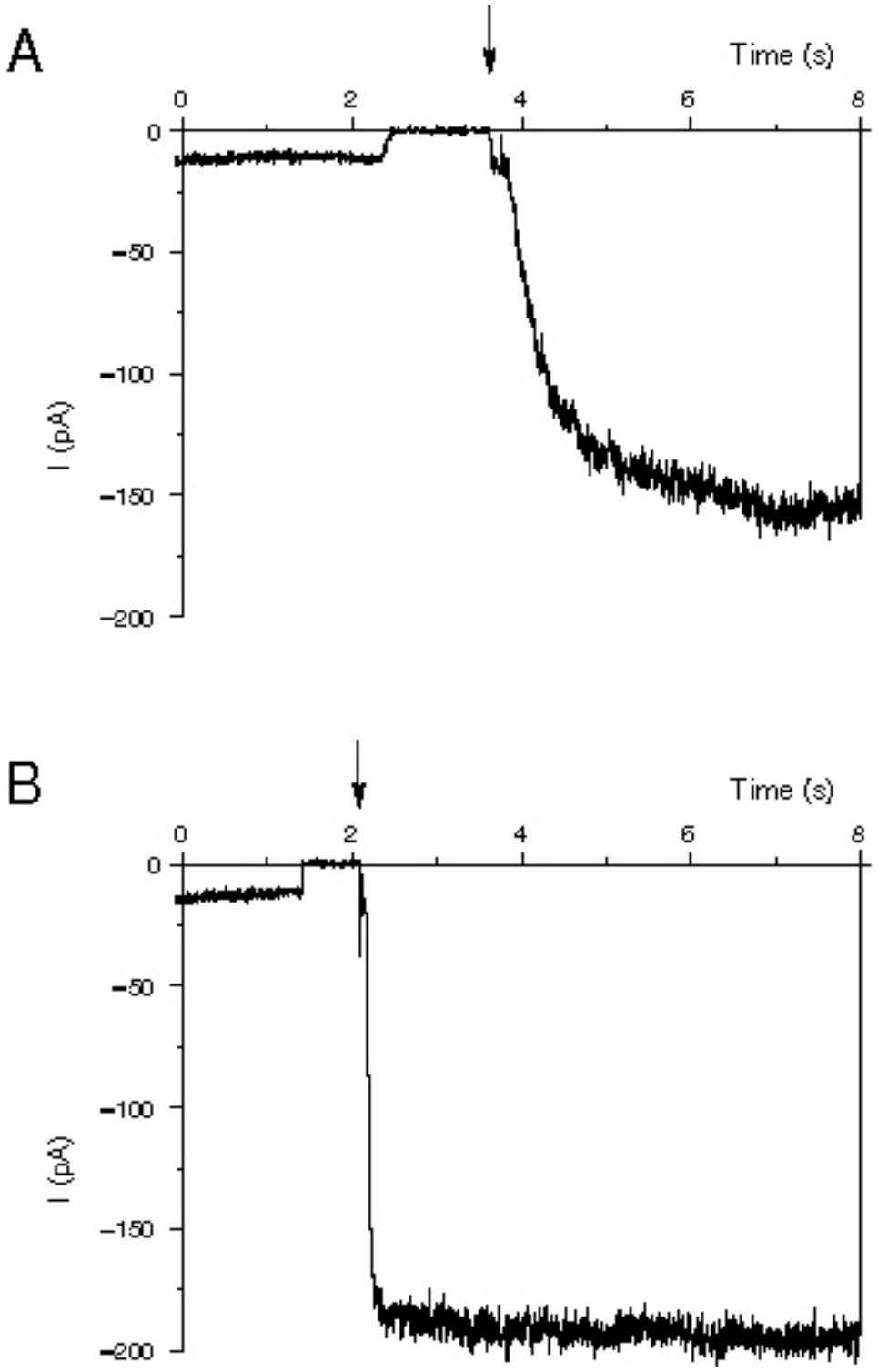
A
Time (s)
0
2
4
6
8
0
−50
−100
−150
−200
I (pA)
B
Time (s)
0
2
4
6
8
0
−50
−100
−150
−200
I (pA)

FIGURE 1

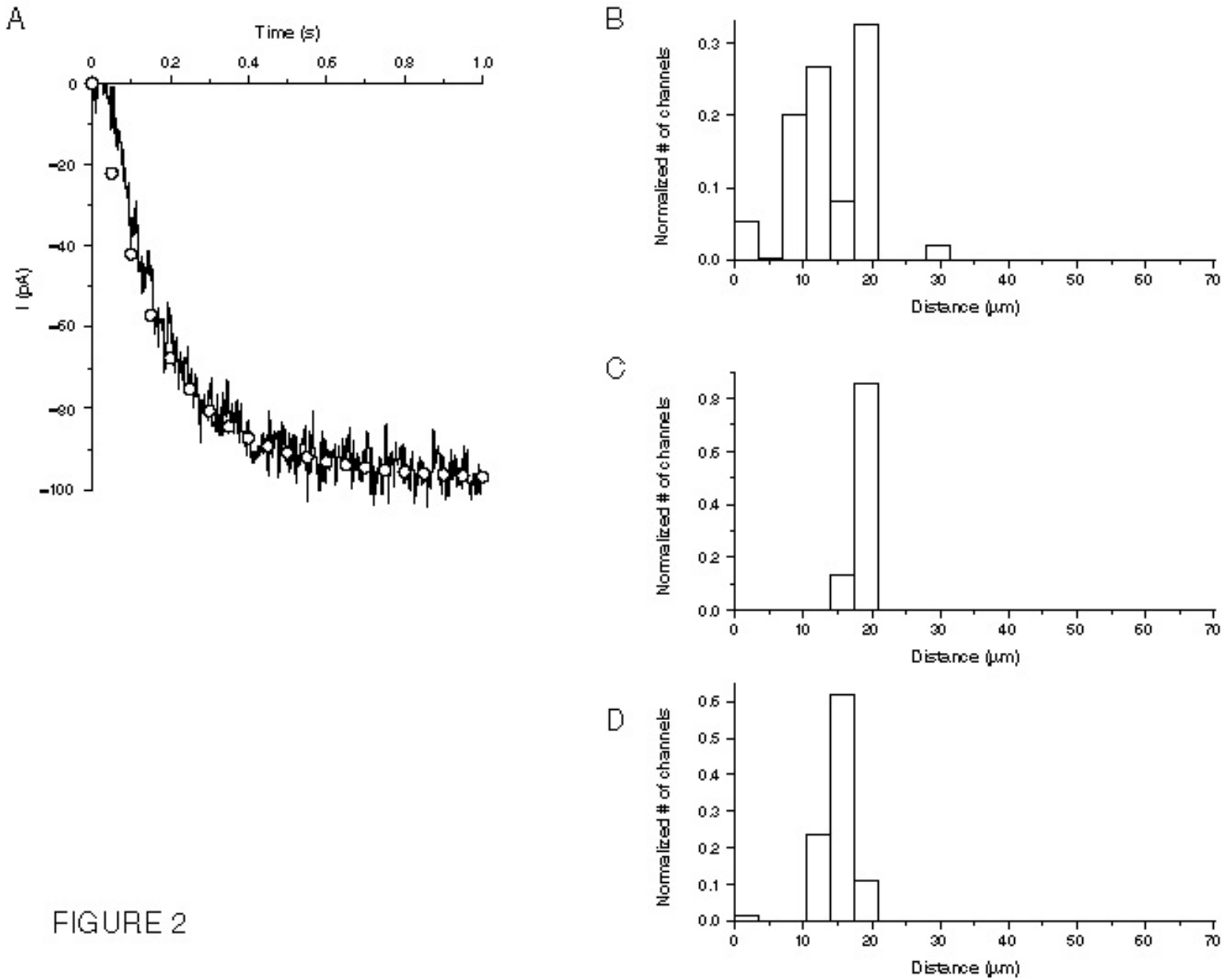
A
Time (s)
0
0.2
0.4
0.6
0.8
1.0
I (pA)
0
-20
-40
-60
-80
-100
B
Normalized # of channels
0.0
0.1
0.2
0.3
Distance (µm)
0
10
20
30
40
50
60
70
C
Normalized # of channels
0.0
0.2
0.4
0.6
0.8
Distance (µm)
D
Normalized # of channels
0.0
0.1
0.2
0.3
0.4
0.5
0.6
Distance (µm)

FIGURE 2

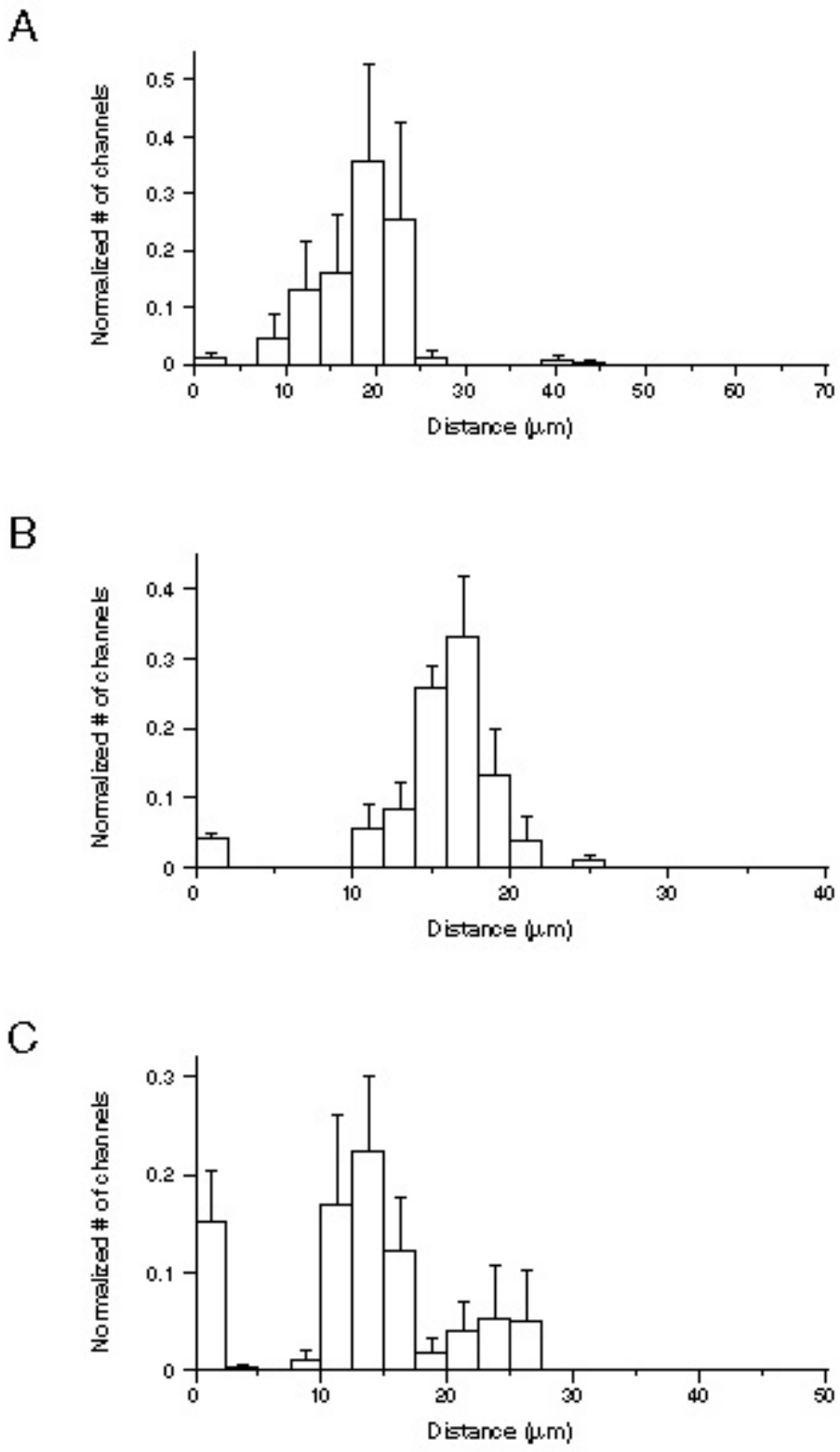
A
Normalized # of channels
0.5
0.4
0.3
0.2
0.1
0
0
10
20
30
40
50
60
70
Distance (µm)
B
Normalized # of channels
0.4
0.3
0.2
0.1
0
0
10
20
30
40
Distance (µm)
C
Normalized # of channels
0.3
0.2
0.1
0
0
10
20
30
40
50
Distance (µm)

FIGURE 3

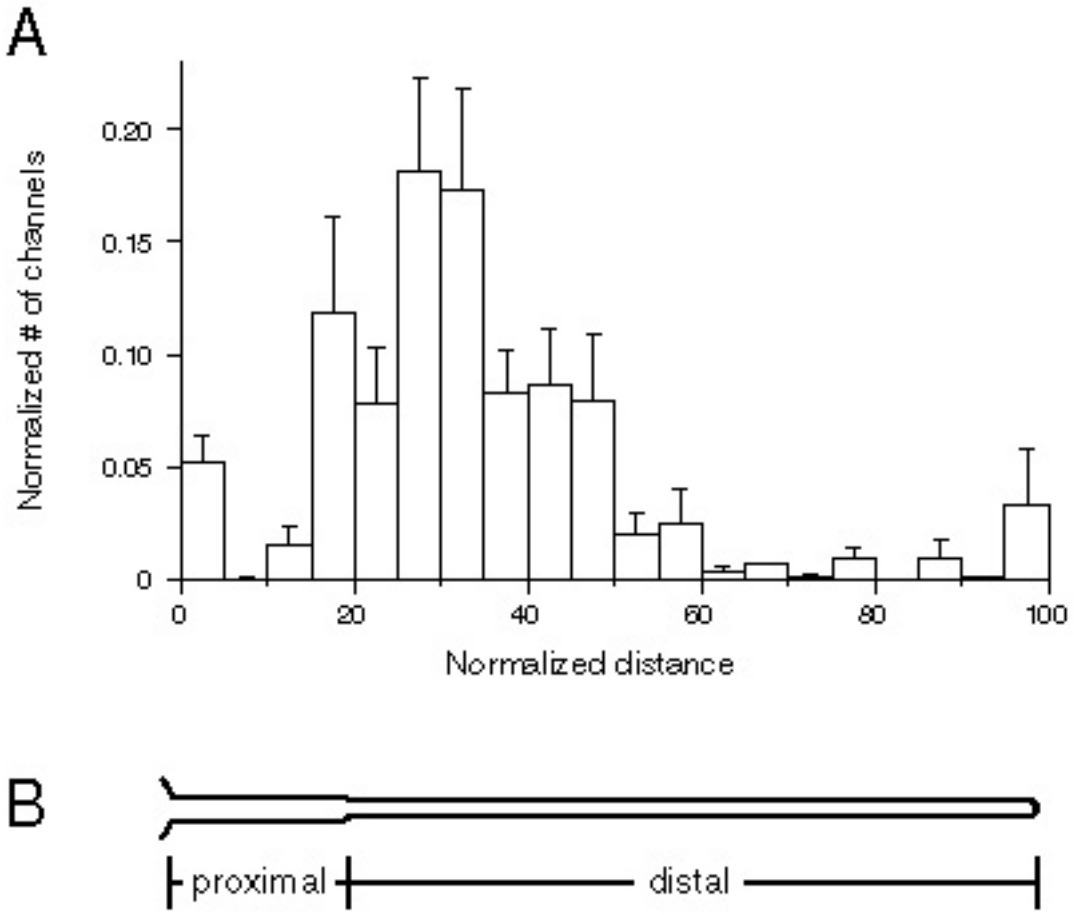
A
Normalized # of channels
0.20
0.15
0.10
0.05
0
0
20
40
60
80
100
Normalized distance
B
proximal
distal

FIGURE 4

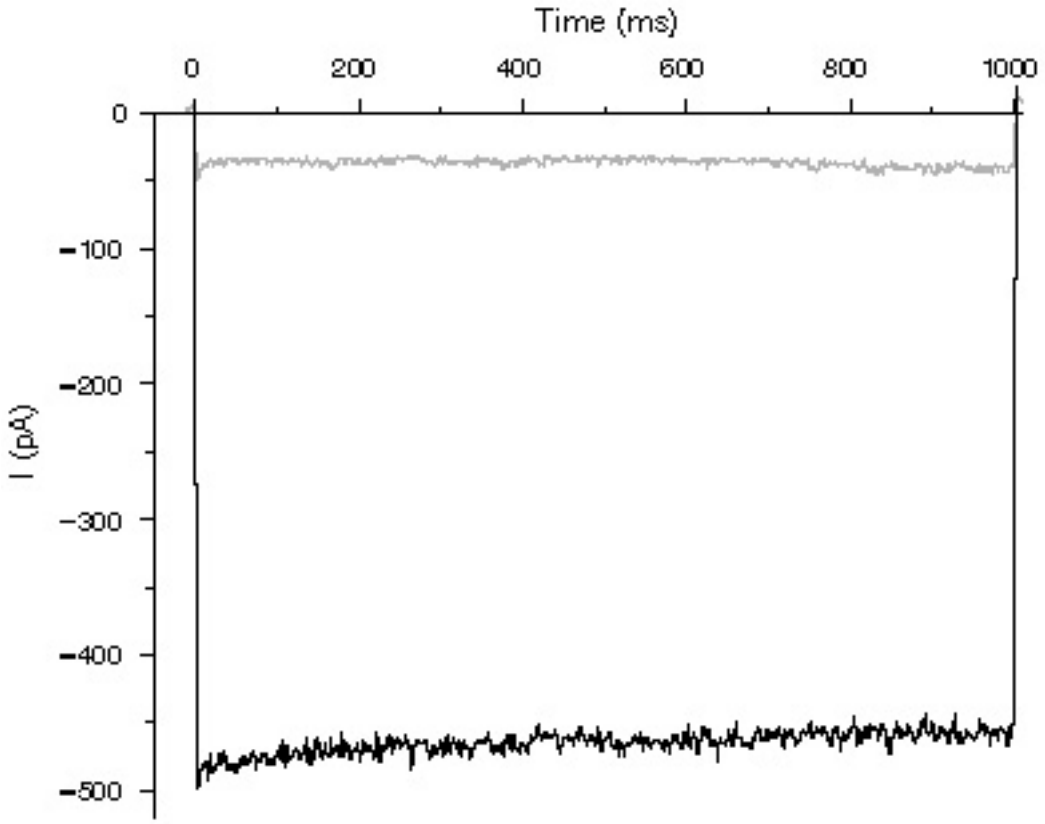

FIGURE 5

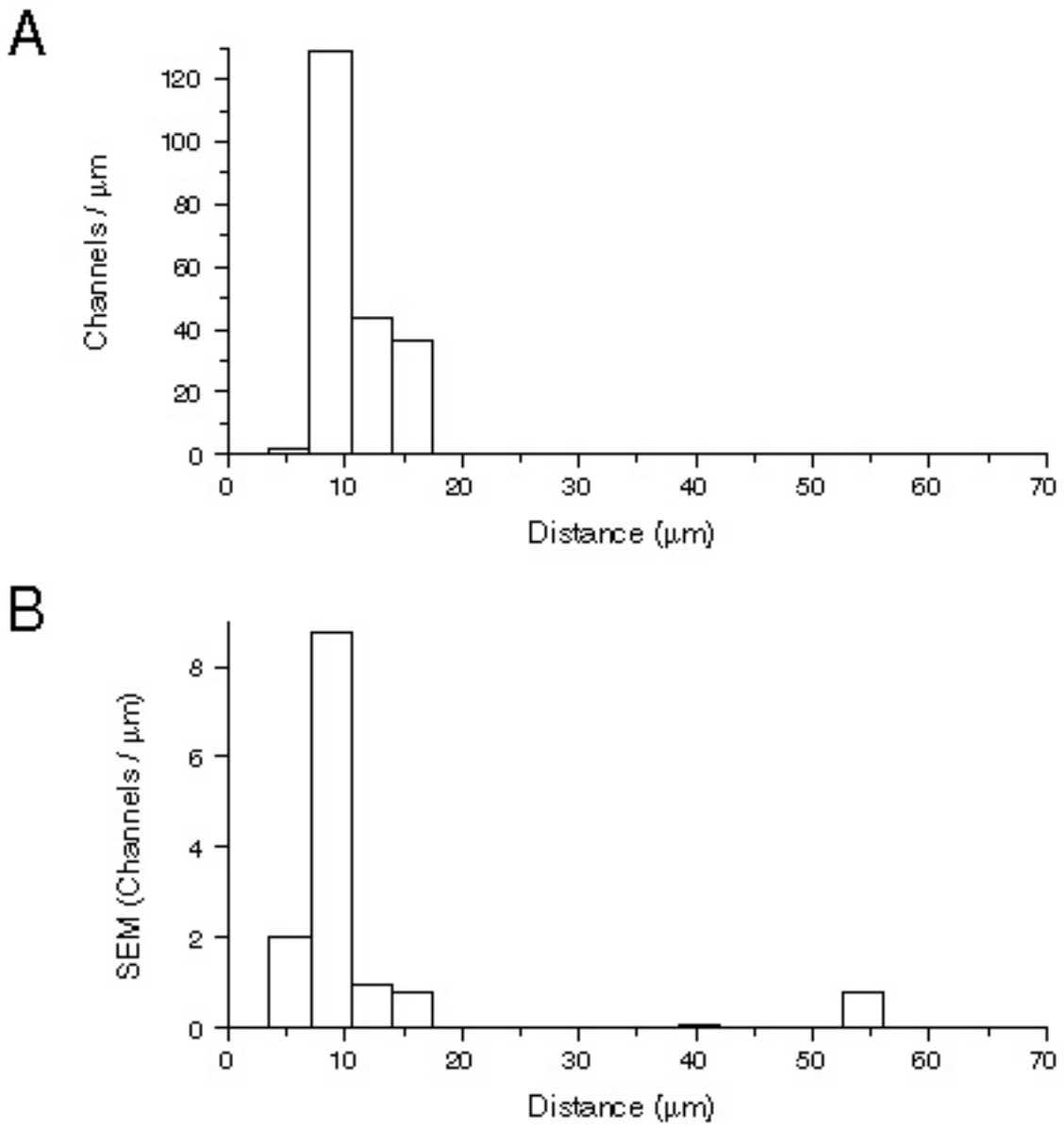
A
Channels / µm
120
100
80
60
40
20
0
0
10
20
30
40
50
60
70
Distance (µm)
B
SEM (Channels / µm)
8
6
4
2
0
0
10
20
30
40
50
60
70
Distance (µm)

FIGURE 6

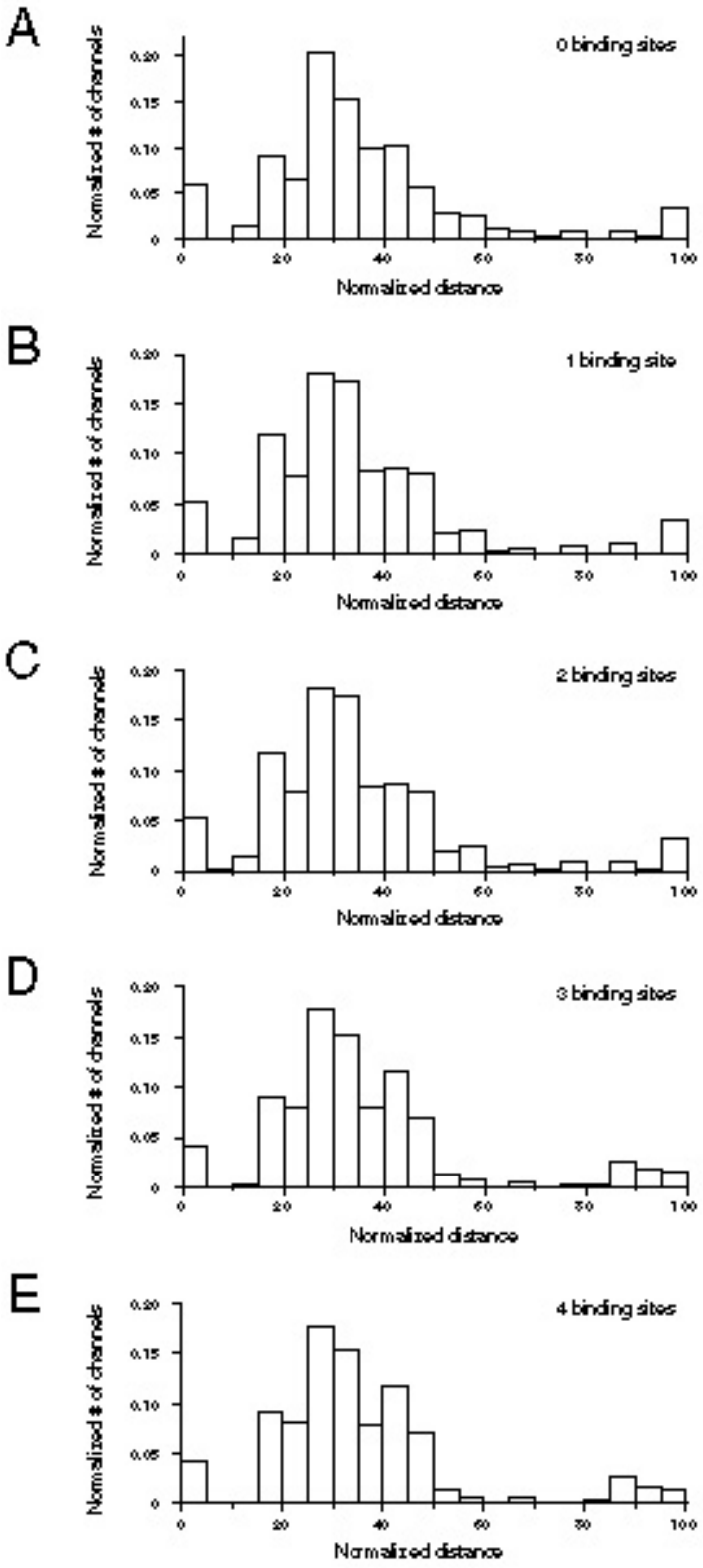
A
0 binding sites
B
1 binding site
C
2 binding sites
D
3 binding sites
E
4 binding sites
Normalized # of channels
Normalized distance
0
0.05
0.10
0.15
0.20
0
20
40
60
80
100

FIGURE 7